Journal of Zhejiang University-SCIENCE A (Applied Physics & Engineering) 2022 23(3):188-207
www.jzus.zju.edu.cn; www.springer.com/journal/11582
E-mail: jzus_a@zju.edu.cn

Research Article

https://doi.org/10.1631/jzus.A2100362

Leap trajectory tracking control based on sliding mode theory for hypersonic gliding vehicle

Kai AN[1], Zhen-yun GUO[1], Wei HUANG[1]✉, Xiao-ping XU[2]

[1]*Science and Technology on Scramjet Laboratory, College of Aerospace Science and Engineering, National University of Defense Technology, Changsha 410073, China*
[2]*Beijing Interdisciplinary Center, National University of Defense Technology, Beijing 100101, China*

Abstract: The aim of this study was to develop robust tracking control schemes for the 3D leap trajectory of hypersonic gliding vehicles using sliding mode theory. A predictor-corrector guidance method was applied to the generation of the reference trajectory, and drag acceleration was selected as the profile of reference tracking. A combined super-twisting sliding mode controller (CST-SMC) is proposed to decrease the tracking error and guarantee the tracking performance in the presence of system nonlinearities compared to three other common controllers: the linear sliding mode controller (L-SMC), global fast terminal sliding mode controller (GFT-SMC), and super-twisting sliding mode controller (ST-SMC). By using the developed controller, the system state of a second-order drag acceleration tracking error system can approach the global fast terminal sliding manifold in finite time. By using the Lyapunov approach, sufficient conditions are deduced to ensure that the tracking performance is obtained for a closed-loop system. Furthermore, we show that the controller is robust to initial uncertain parameters and other perturbations, as validated by simulation results with appropriate gains.

Key words: Predictor-corrector guidance; Drag tracking; Sliding mode control (SMC); Super twisting control

1 Introduction

Hypersonic vehicles have become a hot research field in recent years (Chen et al., 2020, 2021), and their superior maneuverability and penetration will enable great changes in future military combat. However, due to their complex flight environment, strict parameter uncertainty, and strong model nonlinearity, the design of their control systems has become a very challenging research topic. A superior control system is vital for a safe re-entry flight of hypersonic vehicles. To ensure stable flight under complex constraint conditions, the control system must have a rapid response speed and disturbance rejection performance. Hypersonic vehicle control problems are generally divided into two types: trajectory tracking problems and attitude control problems (An et al., 2020). The control of trajectory tracking is the main focus of this paper. Before studying the controller, the desired trajectory is obtained using optimization algorithms, guidance algorithms or path programming methods. For hypersonic gliding vehicles, there are generally two kinds of desired trajectory: quasi equilibrium re-entry trajectories and skipping re-entry trajectories (also known as leap re-entry trajectories). A quasi equilibrium trajectory is smooth and stable without large oscillations, which facilitates better track control and precision (Xu et al., 2012). Skipping gliding flight is generally applied to long range missions, which have serious trajectory oscillation amplitudes, wide flight space, and rapid state change (Wen et al., 2014). Thus, a skipping trajectory requires higher accuracy and robustness in the design of the controller. Since Sänger et al. (1952) first introduced the conceptual scheme, the skipping gliding trajectory has been continuously studied and developed into the "Tsien H. S. trajectory" by Tsien and others (Tsien et al., 1952). After that, the skipping re-entry trajectory of aerospace vehicles (ASVs) has been widely and deeply explored by a large number of scholars (Harpold and Graves Jr,

✉ Wei HUANG, gladrain2001@163.com
Wei HUANG, https://orcid.org/0000-0001-9805-985X

Received July 29, 2021; Revision accepted Oct. 18, 2021;
Crosschecked Jan. 13, 2022

1979; Li et al., 2015; Zhao et al., 2019). In this paper, the challenging skipping trajectory is considered as the reference trajectory for controllers.

Then, a specific controller will be selected to guide the hypersonic vehicle tracking the reference states. Generally, the altitude and velocity sub-systems are constructed as the reference states in the longitudinal plane (Fiorentini et al., 2009; Liu et al., 2015; Zong et al., 2015). However, a drag-based tracking strategy is a typical acceleration guidance method for shuttle entry guidance, and has proved very effective for entry missions (Zhao et al., 2016). Du et al. (2015) proposed a drag-vs-energy profile based on nonlinear model predictive control in which the drag acceleration was considered in the optimization performance index for the entry guidance problem. Zhang et al. (2016) proposed a three-dimensional acceleration profile (TDAP) planner concept that extended the traditional drag planning approach into a 3D drag space. Fu et al. (2021) also designed a drag acceleration-energy profile for generating entry landing footprints. Thus, drag acceleration has been used extensively as the tracking profile in designing standard controllers.

Currently, the conventional control approaches applied in hypersonic vehicles include linear quadratic regulator (LQR) (Lu and Zhou, 2017), feedback linearization control (An et al., 2016), proportional, integral, and derivative (PID) control (Zhao and Li, 2020), fuzzy control (Wu et al., 2017), and back-stepping control (Farrell et al., 2005). Furthermore, sliding mode variable structure control (VSC) shows superior performance in terms of the uncertainty of the system, as a special nonlinear control approach. Utkin (1977) first proposed the method which has been greatly developed in the last 30 years. Research on VSC has focused mainly on the sliding mode surface and reaching law. The sliding mode surface determines the convergence performance of the system, and the reaching law settles the convergence mode. The classic linear sliding hyperplane is generally chosen, where the error system asymptotically converges to zero and the convergence speed can be adjusted by some coefficients. Nevertheless, the system error will not converge to zero in finite time. Yu and Man (2009) designed a novel global fast terminal sliding mode (GFT-SM) to address the poor convergence of the nonlinear sliding mode compared with the linear sliding mode (L-SM) when the system states approached equilibrium in the traditional terminal sliding mode controller (T-SMC). The GFT-SM combines the advantages of the T-SMC and the L-SM controller (L-SMC) so that fast transient convergence can be obtained both at a distance from, and within close range of, the equilibrium. Truong et al. (2021) proposed an integral GFT-SM surface to improve the dynamic performance of the robotic manipulators compared with the terminal sliding mode (T-SM) surface. The GFT-SM controller (GFT-SMC) was also applied in the acceleration autopilot design of the skid-to-turn (STT) nonlinear time-varying missile model (Awad and Wang, 2016). Xiu and Guo (2018) used the quick reaching characteristics and applications of GFT-SMC to overcome the disadvantages of the conventional sliding mode reaching law. So, the GFT-SMC has been developed to improve its performance and has been used in a wide range of applications.

The super-twisting control (STC) algorithm (Levant, 1998) is one of the most powerful second-order continuous sliding mode control algorithms, which drives the sliding variable and its derivative to zero in finite time. This algorithm is widely used to design controllers, observers, and exact differentiators with finite time convergence characteristics (Moreno and Osorio, 2012). Many studies of STC algorithms have been carried out. Yan et al. (2019) proposed an adaptive super-twisting sliding mode controller (ST-SMC) method. The longitudinal model system had less chattering and better robustness. The STC worked better for the formation maneuvers of multiple robots, and dealt well with uncertainties and disturbances with unknown bounds (Zhang et al., 2020). Humaidi and Hasan (2019) presented a robust control algorithm based on an adaptive ST-SMC to guarantee the sliding surface that could reach the equilibrium point and avoid the chattering problem of a 2-DOF (degree of freedom) helicopter.

In this study, the drag acceleration control problem of a 3D trajectory was investigated using four controllers. Firstly, the L-SMC was obtained by combining the L-SM surface and exponential reaching law. Secondly, the GFT-SMC was incorporated and compared with the L-SMC in the application of hypersonic gliding vehicles. Thirdly, ST-SMC was investigated to overcome the chattering effects on controllers that lead to bad performance. Due to the asymptotic convergence of L-SMC and the bad chattering

attenuation of GFT-SMC, a novel combined super-twisting sliding mode controller (CST-SMC) is proposed for guaranteeing that the system can precisely track the reference trajectory. The major contributions of this study are as follows:

1. We consider and deduce a dynamic system of drag tracking error with 3 DOFs.

2. A CST-SMC approach is proposed to improve tracking performance in the total time series compared with the three traditional sliding mode control methods.

3. Generally, in the process of controller performance verification, the system response under various uncertain disturbances (such as parameter perturbation, state error, and environmental disturbance) can best reflect the quality of the controller design and its anti-interference ability. Thus, we discuss the robustness of CST-SMC under parameter perturbation and initial state measurement errors, and verify its effectiveness.

This paper is organized as follows. In Section 2, we describe the generation of the reference trajectory using a predictor-corrector algorithm. In Section 3, we formulate the second-order drag acceleration tracking error system model. Then, in Section 4, we describe the four controllers. Finally, we report the results of the simulation in Section 5.

2 Flight modeling and reference trajectory generation

2.1 Flight modeling

Considering the curvature of the earth and the ground inertial coordinate system, the 3D dynamics of a hypersonic vehicle during the re-entry phase can be precisely described by (Lu, 2014):

$$\begin{aligned}
&\dot{r}=V\sin\gamma,\\
&\dot{\lambda}=\frac{V\cos\gamma\sin\psi}{r\cos\phi},\\
&\dot{\phi}=\frac{V\cos\gamma\cos\psi}{r},\\
&\dot{V}=-D-g\sin\gamma+\omega_e^2 r\cos^2\phi\sin\gamma-\\
&\quad\omega_e^2 r\cos\phi\sin\phi\cos\gamma\cos\psi,\\
&\dot{\gamma}=\frac{1}{V}\left[L\cos\sigma-g\cos\gamma+\frac{V^2\cos\gamma}{r}\right]+\\
&\quad\frac{1}{V}[\omega_e^2 r\cos^2\phi\cos\gamma+2V\omega_e\cos\phi\sin\psi+\\
&\quad\omega_e^2 r\cos\phi\sin\phi\sin\gamma\cos\psi],\\
&\dot{\psi}=\frac{1}{V}\left[\frac{L\sin\sigma}{\cos\gamma}+\frac{V^2\cos\gamma\sin\psi\tan\phi}{r}\right]-\\
&\quad\frac{1}{V}\left[\frac{\omega_e^2 r\cos\phi\sin\phi\cos\psi}{\cos\gamma}+2V\omega_e\sin\phi-\right.\\
&\quad\left.2V\omega_e\cos\phi\tan\gamma\cos\psi\right],
\end{aligned}\tag{1}$$

where r describes the relative distance from the vehicle to the center of the earth, λ and ϕ represent the longitude and latitude, respectively, V is the flight speed, g is the gravitational acceleration, and γ is the flight path angle. The azimuth ψ is defined as the angle of turning, measured clockwise from the local north. σ is the control variable that controls the flight direction in 3D space, and ω_e is a constant representing the angular velocity of the earth. The lift acceleration $L=C_L\rho V^2S/(2m)$ and drag acceleration $D=C_D\rho V^2S/(2m)$ determine the comprehensive flight capability of the vehicle, where m is the mass of vehicle, S is the area of vehicle, C_L and C_D denote the lift coefficient and drag coefficient, respectively, $\rho=\rho_0\exp[-(r-R_e)/h_s]$ is the atmospheric density, ρ_0 is standard atmospheric density, R_e is the earth radius, and h_s is the atmospheric parameter.

2.2 Reference trajectory generation

Considering the trajectory tracking problem, generally, the guidance law or the optimization method is adopted in offline/online trajectory programming in advance for a reference path. Then, the controller is designed to control the vehicle to follow the reference states strictly. Because the predictor-corrector guidance approach has incomparable advantages in online rapid trajectory planning, in this study, this approach was used for a desired, feasible reference that satisfied constraints. The main steps of the predictor-corrector algorithm are as follows (Lu, 2014).

Step 1: Select the angle of attack expressed in the given function and the bank angle which need to be calculated iteratively as the control variables. In every time step, the dynamic equations (Eq. (1)) are integrated to obtain the actual flight distance information from the current state of the vehicle to the terminal conditions, which is called the prediction process.

Step 2: The space motion is divided into two planes because the amplitude and sign of the bank angle need to be solved separately. In the longitudinal

plane, the absolute value of the bank angle will be updated by calculating the difference between the predicted range and the actual range. Meanwhile, constructing the azimuth error corridor for the sign of the bank angle in the lateral plane, the judgment conditions are calculated by the current azimuth and the line-of-sight angle between the vehicle and the target. The final limited re-entry trajectory can be solved when the obtained bank angle is output to the dynamic equation (Eq. (1)). This step is called the rectification process.

Through the prediction process and the rectification process, a satisfactory re-entry leap trajectory under the complex constraint conditions can be solved, and was taken as the reference trajectory of the tracking control in this study. The detailed procedures of this algorithm are described in the following parts.

2.2.1 Constraints transformation

First, the original dynamic equation with time t as the independent variable is transformed into the new model with energy e as the independent variable. The energy expression is defined as

$$e=\frac{\mu}{r}-\frac{V^2}{2}, \tag{2}$$

$$\frac{\mathrm{d}e}{\mathrm{d}t}=DV, \tag{3}$$

where μ is the constant of earth gravitation. The new model can be obtained by combining Eqs. (1) and (3), which can be rewritten as

$$\frac{\mathrm{d}\boldsymbol{x}}{\mathrm{d}e}=f(\boldsymbol{x},\sigma,e),\quad \boldsymbol{x}_0=\boldsymbol{x}\left(e_0\right), \tag{4}$$

where $\boldsymbol{x}$ is the reduced-order state vector, $\boldsymbol{x}_0$ is the initial condition of the state vector, and e_0 is the initial energy.

In the re-entry phase, the vehicle is constrained by several typical inequalities (Eq. (5)) such as path constraints, which include the heating rate $\dot{Q}$, overload n, and dynamic pressure q_a.

$$\begin{aligned}&q_a=0.5\rho V^2\leqslant q_{\max},\\&\dot{Q}=k_Q\sqrt{\rho}\,V^{3.15}\leqslant\dot{Q}_{\max},\\&n=\frac{L}{mg}\leqslant n_{\max},\end{aligned} \tag{5}$$

where $q_{\max}$ is the dynamic-pressure limit, $\dot{Q}_{\max}$ is the heating-rate limit, $k_Q=9.4369\times10^{-5}\times\left(\sqrt{gR_e}\right)^3$, and $n_{\max}$ is the overload limit. Several appropriate terminal conditions, such as terminal velocity limit V_{TAEM}, terminal altitude limit H_{TAEM}, terminal bank angle limit σ_{TAEM}, and terminal flight distance limit S_{TAEM}, also need to be considered (Eq. (6)). It should be pointed out that the subscript TAEM represents terminal area energy management. All the above constraints need to be converted to the range of the bank angle related to velocity.

$$\begin{aligned}&V_{\mathrm{TAEM}}=2000\ \mathrm{m/s},\\&H_{\mathrm{TAEM}}=25\ \mathrm{km},\\&\sigma_{\min}\leqslant\sigma_{\mathrm{TAEM}}\leqslant\sigma_{\max},\\&S_{\mathrm{TAEM}}=50\ \mathrm{km},\end{aligned} \tag{6}$$

where $\sigma_{\max}$ and $\sigma_{\min}$ represent the maximum and minimum values for σ, respectively. The relationship between flight altitude H and flight speed V can be obtained from Eq. (5):

$$\begin{aligned}&H\geqslant H_Q=h_s\ln\left(\frac{k_Q^2\rho_0V^{6.3}}{\dot{Q}_{\max}^2}\right),\\&H\geqslant H_q=h_s\ln\left(\frac{\rho_0V^2}{2q_{\max}}\right),\\&H\geqslant H_n=h_s\ln\left(\frac{C_L\rho_0V^2S}{2mgn_{\max}}\right),\\&H\geqslant\max\left\{H_Q(V),\,H_n(V),\,H_q(V)\right\},\end{aligned} \tag{7}$$

where H_Q, H_q, and H_n are the altitude constraints related to $\dot{Q}_{\max}$, $q_{\max}$, and $n_{\max}$, respectively. Furthermore, the altitude constraints are converted to the ranges of the bank angle amplitudes (σ_Q, σ_n, and σ_q) respectively (Eq. (9)) according to the quasi-equilibrium glide condition (Eq. (8)):

$$\frac{L\cos\sigma}{m}-\left(g-\frac{V^2}{r}\right)=0, \tag{8}$$

$$\sigma\leqslant\max\left\{\sigma_Q(V),\,\sigma_n(V),\,\sigma_q(V)\right\}. \tag{9}$$

2.2.2 Longitudinal guidance

Step 1: To meet the terminal range-to-go, the angle of attack α_0 and bank angle magnitude $\left|\sigma(e)\right|$

profiles are designed as linear piecewise functions, such as Eqs. (10) and (11):

$$\alpha_0=\begin{cases}\alpha_1, & V\geqslant V_1,\\ \alpha_1+\dfrac{\alpha_2-\alpha_1}{V_2-V_1}\left(V-V_1\right), & V_2\leqslant V<V_1,\\ \alpha_2+\dfrac{\alpha_3-\alpha_2}{V_3-V_2}\left(V-V_2\right), & V_3\leqslant V<V_2,\\ \alpha_3, & V<V_3,\end{cases} \tag{10}$$

$$\left|\sigma(e)\right|=\begin{cases}\left|\sigma_{\min}(e)\right|, & \left|\sigma(e)\right|\leqslant\left|\sigma_{\min}(e)\right|,\\ \left|\sigma_{\text{real}}(e)\right|, & \left|\sigma_{\min}(e)\right|<\left|\sigma(e)\right|<\left|\sigma_{\max}(e)\right|,\\ \left|\sigma_{\max}(e)\right|, & \left|\sigma(e)\right|\geqslant\left|\sigma_{\max}(e)\right|,\end{cases} \tag{11}$$

where α_1, α_2, and α_3 are the segmented node variables of the angle of attack model, and they are fixed when the angle of attack model is given. V_1, V_2, and V_3 are the corresponding speed node variables. σ_{real} is an intermediate variable need to be found. The expression of $\left|\sigma(e)\right|$ is

$$\left|\sigma(e)\right|=\sigma_{\text{real}}(e)+\frac{e-e_{\text{real}}}{e_{\text{f}}-e_{\text{real}}}\left(\sigma_{\text{f}}-\sigma_{\text{real}}\right), \tag{12}$$

where e_{f} is the final energy condition, e_{real} is the current energy, and σ_{f} is a sufficient constant.

Step 2: In each guidance cycle, the feasible value of σ_{real} is solved so that the vehicle can be steered from the current states to the final energy conditions e_{f}, and the entry trajectory needs to satisfy the terminal range-to-go constraints:

$$\left|s_{\text{togo}}\left(e_{\text{f}}\right)-s_{\text{f}}^{*}\right|<\varepsilon, \tag{13}$$

where ε is a positive constant, s_{togo} is the range-to-go variable, and s_{f}^{*} represents the desired range-to-go, which is defined as the length of the great circle from the current location to the target:

$$s_{\text{f}}^{*}=\arccos\left[\sin\lambda_{\text{f}}\sin\lambda+\cos\lambda_{\text{f}}\cos\lambda\cos\left(\phi_{\text{f}}-\phi\right)\right], \tag{14}$$

where λ_{f} and ϕ_{f} are the target longitude and latitude, respectively. The updated scheme is approximated by a secant method, where $z(\sigma)=s_{\text{togo}}(e_{\text{f}})-s_{\text{f}}^{*}$, and k_σ is a positive constant that controls the convergence rate:

$$\sigma_{\text{real}}^{(k+1)}=\sigma_{\text{real}}^{(k)}-k_\sigma\frac{z(\sigma_{\text{real}}^{(k)})}{z(\sigma_{\text{real}}^{(k)})-z(\sigma_{\text{real}}^{(k-1)})}(\sigma_{\text{real}}^{(k)}-\sigma_{\text{real}}^{(k-1)}). \tag{15}$$

If the criterion condition (Eq. (13)) is not met, the corrector step seeks to update $\sigma_{\text{real}}(e)$ as the next iteration $\sigma_{\text{real}}^{(k+1)}$ by the secant method using the current energy e_{real}, the kth iteration $\sigma_{\text{real}}^{(k)}$, and the ($k$–1)th iteration $\sigma_{\text{real}}^{(k-1)}$.

2.2.3 Lateral guidance

After σ_{real} has been found, the sign of $\sigma(e)$ is determined by a classic bank-reversal logic in the lateral guidance plane. Assuming that the current longitude is λ_{cur}, the line-of-sight angle ψ_{cur} can be expressed as

$$\psi_{\text{cur}}=\arcsin\frac{\sin(\lambda_{\text{f}}-\lambda_{\text{cur}})\cos\phi_{\text{f}}}{\sin s_{\text{togo}}}. \tag{16}$$

Define the current heading offset $\Delta\psi$ as

$$\Delta\psi=\psi_{\text{V}}-\psi_{\text{cur}}, \tag{17}$$

where ψ_{V} is the actual heading angle.

A velocity-dependent interval segmentation is designed in the form of a piecewise function, where $\Delta\psi_1$ and $\Delta\psi_2$ are the segmented node variables, and so are V_{11} and V_{22}.

$$\Delta\psi=\begin{cases}\Delta\psi_1, & V\geqslant V_{11},\\ \Delta\psi_1+\dfrac{\left(\Delta\psi_1-\Delta\psi_2\right)\cdot\left(V-V_{11}\right)}{V_{11}-V_{22}}, & V_{22}<V<V_{11},\\ \Delta\psi_2, & V\leqslant V_{22}.\end{cases} \tag{18}$$

Once $\Delta\psi$ increases from one direction and exceeds its upper bound $\Delta\psi_{\text{up}}$ or lower bound $\Delta\psi_{\text{down}}$, the bank angle is commanded to change the sign, otherwise, it will remain.

$$\text{sgn}(\sigma^{(k)})=\begin{cases}1, & \Delta\psi>\Delta\psi_{\text{up}},\\ -1, & \Delta\psi<\Delta\psi_{\text{down}},\\ \text{sgn}(\sigma^{(k-1)}), & \text{others},\end{cases} \tag{19}$$

where sgn(σ) is the sign of σ.

Through the above algorithm, the components of the reference states and control curves are obtained (Fig. 1).

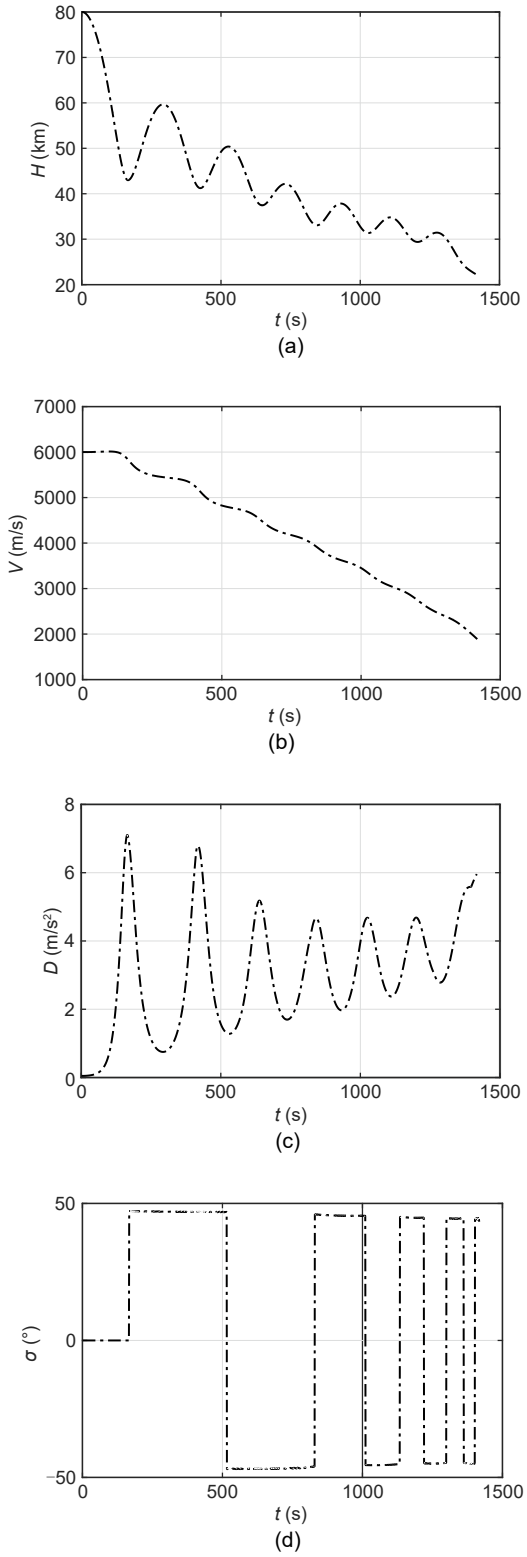

Fig. 1 Components of reference states and control profiles: (a) reference altitude profile; (b) reference velocity profile; (c) reference drag profile; (d) reference control profile

3 Drag tracking problem formulation

Commonly, the design of a tracking controller for a hypersonic vehicle usually focuses on the longitudinal and lateral plane motions. However, there are additional effects that need to be considered in controller design if the dynamic formula is decoupled into the longitudinal plane and the lateral plane. On the one hand, because coupling factors exist in the longitudinal and lateral channels, especially in the process of numerical calculation, the accumulation of errors and complex disturbance terms will increase the complexity of controller design. Simplified dynamic models may also produce inconsistent results. On the other hand, the amount and complexity of controllers require a high computation capacity because they could increase the computational burden of the system.

The trajectory control variable is u=cos σ, and the drag acceleration D is selected as the reference tracking profile. Then, the 3D trajectory of the vehicle can be controlled. The advantages of choosing drag acceleration as the reference instruction are obvious. First and foremost, the tracking problem can be simplified as discussed above, and the drag profile can control both longitudinal and lateral plane motions. Secondly, the drag profile can determine the flight distance to a certain extent. To ensure that the lateral plane motion is close to the desired trajectory, the same strategy as used in the predictor-corrector guidance algorithm is adopted. Therefore, the aim of this study was to design a drag acceleration tracking controller to guarantee that the vehicle can track the reference drag profile rapidly and improve the robustness of the system for the 3D leap trajectory of a hypersonic gliding vehicle.

Define the drag acceleration tracking error e_1 as

$$e_1 = D - D_\mathrm{d}, \tag{20}$$

where D_d is the desired reference drag acceleration. The drag acceleration tracking error dynamics can be obtained by taking the time derivatives of the drag acceleration error in Eq. (20), as follows:

$$\begin{aligned} \dot{e}_1 &= \dot{D} - \dot{D}_\mathrm{d} = e_2, \\ \dot{e}_2 &= \ddot{D} - \ddot{D}_\mathrm{d}. \end{aligned} \tag{21}$$

The expression of drag acceleration is

$$D=\frac{C_D\rho V^2 S}{2m}. \tag{22}$$

Let $B_{\mathrm{fn}}=\dfrac{m}{C_D S}$ be the aerodynamic coefficient, which is taken as a constant. Then, the first derivative of D with respect to time can be obtained from

$$\dot{D}=\frac{1}{2B_{\mathrm{fn}}}\left(\dot{\rho}V^2+2V\rho\dot{V}\right)=f_1. \tag{23}$$

Similarly, the second derivative of D is

$$\begin{aligned}
\ddot{D}&=D\frac{\ddot{\rho}V^2+4\dot{\rho}V\dot{V}+2\rho\dot{V}^2+2\rho V\ddot{V}}{\rho V^2}=\\
&D\left(\frac{\ddot{\rho}}{\rho}+\frac{4\dot{\rho}\dot{V}}{\rho V}+\frac{2\dot{V}^2}{V^2}+\frac{2\ddot{V}}{V}\right)=\\
&D\left(-\frac{\ddot{H}}{h_s}-\frac{\dot{H}}{h_s}\cdot\frac{\dot{\rho}}{\rho}+\frac{4\dot{\rho}\dot{V}}{\rho V}+\frac{2\dot{V}^2}{V^2}+\frac{2\ddot{V}}{V}\right)=\\
&D\left(-\frac{\ddot{H}}{h_s}+\frac{\dot{D}^2}{D^2}-\frac{2\dot{V}^2}{V^2}+\frac{2\ddot{V}}{V}\right)=\\
&D\left(-\frac{3\dot{D}}{V}-\frac{4D^2}{V^2}+\frac{\dot{D}^2}{D^2}-\frac{V^2\cos^2\gamma}{h_s r}+\right.\\
&\left.\frac{g}{h_s}-\frac{\cos\gamma}{h_s}L\cos\sigma\right)+D\left(-\frac{2g}{V^2}L\cos\sigma+\right.\\
&\left.\frac{2g^2\cos^2\gamma}{V^2}-\frac{2g\cos^2\gamma}{r}-\right.\\
&\left.\frac{4gD\sin\gamma+2g^2\sin^2\gamma}{V^2}\right)=f_2+\Delta f_2.
\end{aligned} \tag{24}$$

Considering the flight characteristics of a hypersonic vehicle, the second part Δf_2 of Eq. (24) can be ignored. Also, the flight path angle of the vehicle is always less than 5° from the reference state curves, so we have the approximations $\cos\gamma\approx 1$ and $\sin\gamma\approx\gamma$.

Then, substituting Eqs. (23) and (24) into Eq. (21), the drag acceleration tracking error dynamic equations can be written as

$$\begin{aligned}
\dot{e}_1&=f_1-\dot{D}_{\mathrm{d}},\\
\dot{e}_2&=f_2-\ddot{D}_{\mathrm{d}}+bu,
\end{aligned} \tag{25}$$

where

$$\begin{aligned}
f_1&=\frac{1}{2B_{\mathrm{fn}}}\left(\dot{\rho}V^2+2V\rho\dot{V}\right),\\
f_2&=-\frac{3\dot{D}D}{V}-\frac{4D^3}{V^2}+\frac{\dot{D}^2}{D}-D\frac{V^2\cos^2\gamma}{h_s r}+\frac{gD}{h_s},\\
b&=-\frac{LD}{h_s},\\
u&=\cos\sigma,\quad \sigma\in[-80^\circ,\ 80^\circ].
\end{aligned} \tag{26}$$

The second-order system with respect to the drag acceleration tracking error is constructed, and the goal of controller design is to make the tracking error converge to 0 in finite time.

4 Controller design

4.1 Traditional sliding mode controllers

There are two main assessment indices of controller performance. The first includes rapidity and accuracy, which can ensure that the system reaches the reference point precisely in a limited time. The second is the robustness of the system when subjected to interference by some external disturbances. The sliding mode theory has strong adaptability in the control of nonlinear systems, and comfortably meets these two requirements with reasonable parameters. According to sliding mode theory, the sliding mode motion is usually composed of two stages: the reaching mode motion and the sliding convergence motion. The system can move towards the sliding mode surface no matter which initial state it remains in. That is, when the system reaches the surface $s=0$, it has accomplished the first stage. After that, the controller will force the system to move along the sliding mode surface and converge to the equilibrium point (origin point). The sliding convergence motion is the second stage. Two kinds of sliding mode, L-SM surface and T-SM surface, show better convergence quality with a wide application range. These satisfy the reach conditions $\dot{s}<0$, $s>0$ or $\dot{s}>0$, $s<0$, and guarantee that the system can approach the equilibrium point in finite time along the sliding surface. Yet, an unknown system sliding trajectory limits the evaluation of controller performance. The sliding mode reaching laws, such as the constant velocity reaching law and exponential reaching law, provide a solution to this problem. Therefore, in the following sections we compare and discuss the abilities of the two sliding mode surfaces

and two other approaches to control the leap trajectory of a hypersonic gliding vehicle. Based on the analysis of their characteristics, we propose a combined sliding mode controller to improve global tracking performance.

Note that the following lemmas are needed in the verification of control convergence.

Lemma 1 Considering a nonlinear sliding mode surface s,

$$s=\dot{e}_s+\alpha e_s+\beta e_s^{\frac{p}{q}},\quad \alpha,\ \beta>0,\ p,\ q\ (p<q), \tag{27}$$

where e_s is the error variable, and α, β, p, and q are all constants. If the condition $s=0$ has been satisfied, the equilibrium point of the system is globally finite-time stable in time t_s:

$$t_{\mathrm{s}}=t_{\mathrm{r}}+\frac{q}{\alpha(q-p)}\ln\frac{\alpha\left(e_s\left(t_{\mathrm{r}}\right)\right)^{\frac{q-p}{q}}+\beta}{\beta}, \tag{28}$$

where t_r is the reach time in which the system moves from arbitrary initial states to the sliding surface $s=0$.

Proof The expression of convergence time can be obtained by solving the differential equation $s=0$ analytically. As soon as the system reaches the sliding mode surface from any initial states, Eq. (27) can be written as

$$\dot{e}_s+\alpha e_s+\beta e_s^{\frac{p}{q}}=0. \tag{29}$$

Dividing both sides by $e_s^{\frac{p}{q}}$ yields

$$e_s^{-\frac{p}{q}}\dot{e}_s+\alpha e_s^{1-\frac{p}{q}}=-\beta. \tag{30}$$

Letting $y=e_s^{1-\frac{p}{q}}$, and deducing $\frac{\mathrm{d}y}{\mathrm{d}t}=\frac{q-p}{q}e_s^{-\frac{p}{q}}\dot{e}_s$, Eq. (30) can be rewritten as

$$\frac{\mathrm{d}y}{\mathrm{d}t}+\frac{q-p}{q}\alpha y=-\frac{q-p}{q}\beta. \tag{31}$$

Obviously, Eq. (31) is a first-order differential equation, with the common form of

$$\frac{\mathrm{d}y}{\mathrm{d}t}+P(x)y=Q(x), \tag{32}$$

where $P(x)$ and $Q(x)$ are polynomial expressions, and x represents the arbitrary variable. Then, the general solution is

$$y=\mathrm{e}^{-\int P(x)\mathrm{d}x}\left(\int Q(x)\ \mathrm{e}^{\int P(x)\mathrm{d}x}\mathrm{d}x+C\right), \tag{33}$$

where C is a constant.

Substituting the terms corresponding to $P(x)$ and $Q(x)$ in Eq. (31) into Eq. (33), we can obtain:

$$\begin{aligned}
y&=\mathrm{e}^{-\int_0^t\frac{q-p}{q}\alpha\mathrm{d}t}\left[\int_0^t\left(-\frac{q-p}{q}\right)\beta\mathrm{e}^{\int_0^t\frac{q-p}{q}\alpha\mathrm{d}t}\mathrm{d}t+C\right]=\\
&\mathrm{e}^{-\int_0^t\frac{q-p}{q}\alpha\mathrm{d}t}\left[\int_0^t\left(-\frac{q-p}{q}\right)\beta\mathrm{e}^{\frac{q-p}{q}\alpha t}\mathrm{d}t+C\right]=\\
&\mathrm{e}^{-\frac{q-p}{q}\alpha t}\left[-\frac{q-p}{q}\beta\frac{q}{(q-p)\alpha}\mathrm{e}^{\frac{q-p}{q}\alpha t}\Big|_0^t+y(0)\right]=\\
&-\frac{\beta}{\alpha}+\frac{\beta}{\alpha}\mathrm{e}^{-\frac{q-p}{q}\alpha t}+y(0)\ \mathrm{e}^{-\frac{q-p}{q}\alpha t}.
\end{aligned} \tag{34}$$

Then, for $e_s=0$, $y=0$, and $t=t_s$,

$$\begin{aligned}
&\frac{\beta}{\alpha}\mathrm{e}^{-\frac{q-p}{q}\alpha t_{\mathrm{s}}}+y(0)\ \mathrm{e}^{-\frac{q-p}{q}\alpha t_{\mathrm{s}}}=\frac{\beta}{\alpha},\\
&\left(\frac{\beta}{\alpha}+y(0)\right)\mathrm{e}^{-\frac{q-p}{q}\alpha t_{\mathrm{s}}}=\frac{\beta}{\alpha},\\
&\left(1+\frac{\alpha}{\beta}y(0)\right)=\mathrm{e}^{\frac{q-p}{q}\alpha t_{\mathrm{s}}},
\end{aligned} \tag{35}$$

where $y(0)=e_s(0)^{\frac{q-p}{q}}$. Hence, the total convergence time is determined by

$$t_{\mathrm{s}}=\frac{q}{\alpha(q-p)}\ln\frac{\alpha e_s(0)^{\frac{q-p}{q}}+\beta}{\beta}. \tag{36}$$

The system will reach the balanced states in finite time through the appropriate parameters α, β, p, and q.

Lemma 2 The non-Lipschitz continuous nonlinear system is given as

$$\begin{aligned}
&\dot{\boldsymbol{x}}_{\mathrm{L}}=f\left(\boldsymbol{x}_{\mathrm{L}},\ t\right),\\
&\boldsymbol{x}_{\mathrm{L}}\left(t_0\right)=\boldsymbol{x}_{\mathrm{L0}},
\end{aligned} \tag{37}$$

where $\boldsymbol{x}_{\mathrm{L}}$ is the continuous nonlinear system vector, and t_0 is the initial time. Suppose there exists a continuous and differentiable function $V_{\mathrm{L}}(\boldsymbol{x}_{\mathrm{L}})$ and real numbers $\alpha_{\mathrm{V}}>0$ and $0<\beta_{\mathrm{V}}<1$, and the conditions $V_{\mathrm{L}}\left(\boldsymbol{x}_{\mathrm{L}}\right)>0$ and $\dot{V}_{\mathrm{L}}\left(\boldsymbol{x}_{\mathrm{L}}\right)+\alpha_{\mathrm{V}}V_{\mathrm{L}}^{\beta_{\mathrm{V}}}\left(\boldsymbol{x}_{\mathrm{L}}\right)\leqslant 0$ are satisfied. Then, the origin is a finite-time stable equilibrium of Eq. (37). If T_{s} is the settling time, then for all $\boldsymbol{x}_{\mathrm{L}}$ in some open neighborhood of the origin,

$$T_{\mathrm{s}}\leqslant \frac{V_{\mathrm{L}}^{1-\beta_{\mathrm{V}}}\left(\boldsymbol{x}_{\mathrm{L}}\right)}{\alpha_{\mathrm{V}}\left(1-\beta_{\mathrm{V}}\right)}. \tag{38}$$

Once $t\geqslant T_{\mathrm{s}}$, $s=\dot{s}=0$.

Lemma 3 For the system,

$$\begin{aligned}\dot{x}_1&=x_2-k_{x1}\left|x_1\right|^{\frac{1}{2}}\operatorname{sgn}\left(x_1\right),\\ \dot{x}_2&=-k_{x2}\operatorname{sgn}\left(x_1\right),\end{aligned} \tag{39}$$

where k_{x1} and k_{x2} are constants. $x_1, x_2\in\mathbb{R}$ indicates the system states are continuous. Then, the system is finite-time stable.

4.1.1 Linear sliding mode controller (L-SMC)

Let the L-SM surface be chosen in terms of drag acceleration error e_1 such that

$$s=ce_1+\dot{e}_1, \tag{40}$$

where c is a constant.

Differentiate Eq. (40),

$$\dot{s}=ce_2+\dot{e}_2=ce_2+\left(f_2-\ddot{D}_{\mathrm{d}}+bu\right). \tag{41}$$

To ensure the sliding mode surface can converge to zero in finite time, the following reaching law is considered:

$$\dot{s}=-\eta\operatorname{sgn}(s)-k_s s,\quad \eta,\ k_s>0, \tag{42}$$

where η and k_s are constants. Substituting Eq. (42) into Eq. (41), the controller u can be obtained:

$$u=-\frac{1}{b}(f_2-\ddot{D}_{\mathrm{d}}+ce_2+\eta\operatorname{sgn}(s)+k_s s). \tag{43}$$

Theorem 1 For the dynamic model Eq. (1) of a hypersonic gliding vehicle, if the L-SM manifold is chosen as in Eq. (40), the reaching law is Eq. (42), and the continuous L-SMC is designed as Eq. (43), then the tracking error e_1 will converge to zero as time $t\to\infty$, and the state variables will converge to their desired values.

Proof Choose the following Lyapunov function candidate V_{L}:

$$V_{\mathrm{L}}=\frac{1}{2}s^2. \tag{44}$$

Derivate Eq. (44) using Eq. (41),

$$\dot{V}_{\mathrm{L}}=s\dot{s}=s\left[ce_2+\left(f_2-\ddot{D}_{\mathrm{d}}+bu\right)\right]. \tag{45}$$

Substituting Eq. (43) into Eq. (45) yields,

$$\dot{V}_{\mathrm{L}}=s\left(-\eta\operatorname{sgn}(s)-k_s s\right)=-\eta|s|-k_s s^2. \tag{46}$$

Since $\eta,\ k_s>0$ in Eq. (46), and $\dot{V}_{\mathrm{L}}$ is negative definite, then $\dot{V}_{\mathrm{L}}\leqslant 0$, which implies that the system will reach the sliding mode surface in finite time. Once the condition $s=0$ is satisfied, the following equation can be obtained:

$$ce_1+\dot{e}_1=0. \tag{47}$$

Solving Eq. (47) analytically,

$$e_1(t)=e_1(0)\ \mathrm{e}^{-ct}. \tag{48}$$

Then, the tracing error e_1 will converge to zero as time $t\to\infty$ with a convergence rate c. Note that the system arrives asymptotically.

4.1.2 Global fast terminal sliding mode controller (GFT-SMC)

Define the following sliding mode manifold:

$$s=\dot{e}_1+\alpha e_1+\beta e_1^{\frac{p}{q}},\quad \alpha,\ \beta>0,\ p,\ q\ (p<q). \tag{49}$$

The same reaching law is applied:

$$\dot{s}=-\eta\operatorname{sgn}(s)-k_s s,\quad \eta,\ k_s>0. \tag{50}$$

Then, the GFT-SMC law can be deduced from Eq. (50) and the derivative of Eq. (49):

$$u=-\frac{1}{b}\left(f_2-\ddot{D}_{\mathrm{d}}+\alpha\dot{e}_1+\beta\frac{p}{q}e_1^{\frac{p}{q}-1}\dot{e}_1+\eta\,\mathrm{sgn}(s)+k_s s\right). \tag{51}$$

Theorem 2 For system Eq. (1) and tracking error dynamic Eq. (25) with the GFT-SM surface Eq. (49), the designed controller Eq. (51) will force the states e_1 and e_2 to converge to zero in finite time, and then the system states will be consistent with the desired states.

Proof Taking the time derivative of the surface s, and applying the control law given by Eq. (51), we have the following deduction:

$$\begin{aligned}\dot{s}&=\dot{e}_2+\alpha e_2+\beta\frac{p}{q}e_1^{\frac{p}{q}-1}e_2=\\&f_2-\ddot{D}_{\mathrm{d}}+bu+\alpha e_2+\beta\frac{p}{q}e_1^{\frac{p}{q}-1}e_2=\\&-\eta\,\mathrm{sgn}(s)-k_s s.\end{aligned} \tag{52}$$

Let the Lyapunov function candidate be such that:

$$V_{\mathrm{L}}=\frac{1}{2}s^2. \tag{53}$$

Differentiating V_{L} with respect to time and substituting Eq. (52) yields

$$\dot{V}_{\mathrm{L}}=s\left(-\eta\,\mathrm{sgn}(s)-k_s s\right)=-\eta|s|-k_s s^2. \tag{54}$$

It is clear from Eq. (54) that $\dot{V}_{\mathrm{L}}\leqslant 0$ when η, $k_s>0$. Therefore, the system can reach the sliding surface in finite time under the reaching law Eq. (52). Once the system remains on the sliding mode surface, the following dynamic is guaranteed with reasonable parameters α, β, p, and q:

$$\dot{e}_1+\alpha e_1+\beta e_1^{\frac{p}{q}}=0. \tag{55}$$

From Lemma 1, this dynamic ensures the finite-time convergence of e_1 and e_2 to zero in time t_s. Furthermore, the system states will be consistent with the desired states.

4.1.3 Super-twisting sliding mode controller (ST-SMC)

The ST-SMC is a kind of second-order control algorithm, which differs from the exponential reaching law used in Sections 4.1.1 and 4.1.2. The algorithm consists of two parts: the discontinuous time differentiation of the sliding mode variable, and the continuous function in terms of the sliding mode variable. System chattering can be effectively suppressed by this algorithm compared with other first-order sliding mode control laws, and the robustness of traditional sliding mode controllers can be retained.

Considering the global fast terminal sliding manifold in terms of e_1 and e_2:

$$s=\dot{e}_1+\alpha e_1+\beta e_1^{\frac{p}{q}},\quad \alpha,\,\beta>0,\,p,\,q\,(p<q). \tag{56}$$

Then, the finite time ST-SMC is designed as

$$\begin{aligned}&u=-\frac{1}{b}(f_2-\ddot{D}_{\mathrm{d}}+\alpha\dot{e}_1+\beta\frac{p}{q}e_1^{\frac{p}{q}-1}\dot{e}_1+u_{\mathrm{n}}),\\&u_{\mathrm{n}}=-\upsilon|s|^{\frac{1}{2}}\mathrm{sgn}(s)+u_1,\\&\dot{u}_1=-\omega\,\mathrm{sgn}(s),\end{aligned} \tag{57}$$

where $\upsilon>0$ and $\omega>0$ are constants. The reaching condition is $s\dot{s}<0$. Substituting Eqs. (56) and (57) into it yields:

$$s\dot{s}=s\left(\ddot{e}_1+\alpha\dot{e}_1+\beta\frac{p}{q}e_1^{\frac{p}{q}-1}\dot{e}_1\right)=su_{\mathrm{n}}<0. \tag{58}$$

Thus, the system satisfies the reaching conditions from any initial state to the surface.

Theorem 3 For the dynamical vehicle model Eq. (1) and the sliding surface Eq. (56), the system tracking errors Eq. (25) will converge to zero eventually, and the vehicle will be situated at the desired point in finite time by controller Eq. (57).

Proof (1) Prove the sliding mode variable s will converge in finite time.

Taking the time derivative of Eq. (56), we can obtain:

$$\begin{aligned}\dot{s}&=\dot{e}_2+\alpha e_2+\beta\frac{p}{q}e_1^{\frac{p}{q}-1}e_2=\\&f_2-\ddot{D}_{\mathrm{d}}+bu+\alpha e_2+\beta\frac{p}{q}e_1^{\frac{p}{q}-1}e_2.\end{aligned} \tag{59}$$

Substituting Eq. (57) into Eq. (59), we can obtain:

$$\dot{s}=u_{\mathrm{n}}. \tag{60}$$

According to Lemma 3, the sliding mode variables can converge to zero in finite time.

(2) Verify the convergence of the drag tracking error in finite time.

Once the system reaches the sliding mode surface, the condition will be satisfied, then

$$\dot{e}_1+\alpha e_1+\beta e_1^{\frac{p}{q}}=0. \tag{61}$$

From Lemma 1, this dynamic ensures the finite-time convergence of e_1 and e_2 to zero in time t_s. Furthermore, the system states will be consistent with the desired states. The proof is finished.

4.2 Combined super-twisting sliding mode controller (CST-SMC)

Considering the characteristics of the exponential reaching law and super-twisting sliding mode algorithm (see Remarks 1 and 2 for details), a novel combined finite time super-twisting sliding mode controller (CST-SMC) is designed, which also adopts the GFT-SM surface:

$$s=\dot{e}_1+\alpha e_1+\beta e_1^{\frac{p}{q}},\quad \alpha,\ \beta>0,\ p,\ q\ (p<q). \tag{62}$$

The CST-SMC is designed as

$$\begin{aligned} u=&-\frac{1}{b}\left(f_2-\ddot{D}_{\mathrm{d}}+\alpha\dot{e}_1+\beta\frac{p}{q}e_1^{\frac{p}{q}-1}\dot{e}_1+\right.\\ &\left.\eta\,\mathrm{sgn}(s)+k_s s+u_{\mathrm{n}}\right),\\ u_{\mathrm{n}}=&-\upsilon|s|^{\frac{1}{2}}\mathrm{sgn}(s)+u_1,\\ \dot{u}_1=&-\omega\,\mathrm{sgn}(s)-k_2u_1, \end{aligned} \tag{63}$$

where $k_2>0$ is a constant.

Theorem 4 For the hypersonic gliding vehicle dynamic system Eq. (1), the T-SM surface Eq. (62) and the CST-SMC Eq. (63) can ensure that all the states information can track the reference trajectories in finite time.

Proof (1) Prove the system error can reach the sliding manifold $s=0$ in finite time.

Substituting Eq. (63) into Eq. (25), we have the detailed expression:

$$\dot{e}_1=e_2,$$

$$\dot{e}_2=-\alpha\dot{e}_1-\beta\frac{p}{q}e_1^{\frac{p}{q}-1}\dot{e}_1-\eta\,\mathrm{sgn}(s)-k_s s+u_{\mathrm{n}}. \tag{64}$$

The novel reaching law is designed as

$$\begin{aligned} \dot{s}=&-\eta\,\mathrm{sgn}(s)-k_s s-\upsilon|s|^{\frac{1}{2}}\mathrm{sgn}(s)+u_1,\\ \dot{u}_1=&-\omega\,\mathrm{sgn}(s)-k_2u_1. \end{aligned} \tag{65}$$

Dividing Eq. (65) into two sub-systems,

$$\dot{s}=-\eta\,\mathrm{sgn}(s)-k_s s, \tag{66}$$

$$\begin{aligned} \dot{s}=&-\upsilon|s|^{\frac{1}{2}}\mathrm{sgn}(s)+u_1,\\ \dot{u}_1=&-\omega\,\mathrm{sgn}(s)-k_2u_1. \end{aligned} \tag{67}$$

The exponential approach term $\dot{s}=-k_s s$ in system Eq. (66) has the solution $s=s(0)\,\mathrm{e}^{-k_s t}$, which implies that progress towards the sliding surface is a gradual process and does not satisfy the condition of finite-time arrival. In this case, if a constant speed reaching term is included, the reaching speed will decrease to η as soon as s is close to zero, so the finite-time arrival of the system can be guaranteed.

We discuss mainly the stability of system Eq. (67). Define a 2D vector $\boldsymbol{w}$:

$$\boldsymbol{w}=[\,w_1\quad w_2\,]^{\mathrm{T}}=\left[\,|s|^{\frac{1}{2}}\mathrm{sgn}(s)\quad u_1\,\right]^{\mathrm{T}}. \tag{68}$$

Derivate Eq. (68) according to the property of matrix derivation:

$$\dot{\boldsymbol{w}}=\frac{1}{|w_1|}\boldsymbol{A}\boldsymbol{w}, \tag{69}$$

where $\boldsymbol{A}=\begin{bmatrix}-\dfrac{\upsilon}{2} & \dfrac{1}{2}\\ -\omega & -k_2|w_1|\end{bmatrix}$. Choose the Lyapunov function

$$V_{\mathrm{L}}=\boldsymbol{w}^{\mathrm{T}}\boldsymbol{P}\boldsymbol{w}, \tag{70}$$

where $\boldsymbol{P}=\begin{bmatrix}\upsilon^2+1 & -\upsilon\\ -\upsilon & \omega+1\end{bmatrix}$ is a positive definite symmetric constant matrix.

$$\dot{V}_{\mathrm{L}}=\frac{2}{\left|w_1\right|}\boldsymbol{w}^{\mathrm{T}}\boldsymbol{P}\boldsymbol{A}\boldsymbol{w}=-\frac{1}{\left|w_1\right|}\boldsymbol{w}^{\mathrm{T}}\boldsymbol{Q}\boldsymbol{w}, \tag{71}$$

where $\boldsymbol{P}$, $\boldsymbol{A}$, and $\boldsymbol{Q}$ are related by

$$\boldsymbol{A}^{\mathrm{T}}\boldsymbol{P}+\boldsymbol{P}\boldsymbol{A}=-\boldsymbol{Q}. \tag{72}$$

Suppose $\lambda_{\min}(\boldsymbol{Q})$ is the minimum eigenvalue about matrix $\boldsymbol{Q}$, then the following inequality holds:

$$\lambda_{\min}(\boldsymbol{Q})\left\|\boldsymbol{w}\right\|^2\leqslant\boldsymbol{w}^{\mathrm{T}}\boldsymbol{Q}\boldsymbol{w}. \tag{73}$$

Substituting Eq. (73) into Eq. (71), then

$$\dot{V}_{\mathrm{L}}=-\frac{1}{\left|w_1\right|}\boldsymbol{w}^{\mathrm{T}}\boldsymbol{Q}\boldsymbol{w}\leqslant-\frac{1}{\left|w_1\right|}\lambda_{\min}(\boldsymbol{Q})\left\|\boldsymbol{w}\right\|^2. \tag{74}$$

Similarly, we suppose $\lambda_{\min}(\boldsymbol{P})$ and $\lambda_{\max}(\boldsymbol{P})$ are the minimum eigenvalue and maximum eigenvalue about matrix $\boldsymbol{P}$, respectively, so the inequalities can be obtained from Eq. (70):

$$V_{\mathrm{L}}=\boldsymbol{w}^{\mathrm{T}}\boldsymbol{P}\boldsymbol{w}\leqslant\lambda_{\max}(\boldsymbol{P})\left\|\boldsymbol{w}\right\|^2, \tag{75}$$

$$\left|w_1\right|\leqslant\left\|\boldsymbol{w}\right\|\leqslant\frac{V_{\mathrm{L}}^{\frac{1}{2}}}{\lambda_{\min}^{\frac{1}{2}}(\boldsymbol{P})}. \tag{76}$$

In conclusion, we have the final expression reflecting the properties of the Lyapunov function:

$$\dot{V}_{\mathrm{L}}=-\frac{1}{\left|w_1\right|}\boldsymbol{w}^{\mathrm{T}}\boldsymbol{Q}\boldsymbol{w}\leqslant-\frac{\lambda_{\min}^{\frac{1}{2}}(\boldsymbol{P})\lambda_{\min}(\boldsymbol{Q})}{\lambda_{\max}(\boldsymbol{P})}V_{\mathrm{L}}^{\frac{1}{2}}. \tag{77}$$

According to Lemma 2, the system is finite-time stable if the parameters υ, ω, and k_2 satisfy the Lipschitz conditions. The convergence time T_2 is

$$T_2\leqslant\frac{2\lambda_{\max}(\boldsymbol{P})V_{\mathrm{L}}^{\frac{1}{2}}(x)}{\lambda_{\min}^{\frac{1}{2}}(\boldsymbol{P})\lambda_{\min}(\boldsymbol{Q})}. \tag{78}$$

Suppose the convergence time (T_1) of system Eq. (66) meets the expression $T_1\leqslant T_{\mathrm{c}}$ (where T_{c} is the fixed time), and then the original system Eq. (65) has the reaching time T_{r}:

$$T_{\mathrm{r}}=T_1+T_2\leqslant T_{\mathrm{c}}+\frac{2\lambda_{\max}(\boldsymbol{P})V_{\mathrm{L}}^{\frac{1}{2}}(x)}{\lambda_{\min}^{\frac{1}{2}}(\boldsymbol{P})\lambda_{\min}(\boldsymbol{Q})}. \tag{79}$$

The system will meet the condition $s=0$ because of Eq. (79).

(2) Verify the drag acceleration error converges to zero in finite time.

Once the error variables e_1 and e_2 reach the sliding mode surface $s=\dot{s}=0$, Eq. (62) can be further represented as

$$\dot{s}=\dot{e}_2+\alpha e_2+\beta\frac{p}{q}e_1^{\frac{p}{q}-1}e_2=0. \tag{80}$$

By Lemma 1, the above system Eq. (64) will show finite-time stability to the equilibrium point.

Remark 1 The GFT-SM surface has unique advantages over the L-SM surface. It can ensure that the system reaches the sliding mode surface rapidly and guides the system to converge to the origin point in finite time, compared with the asymptotic convergence of L-SM. Also, the small enough index p/q constricts system movement within a small neighborhood of the sliding surface. Moreover, it is more robust in response to system perturbation and disturbance.

Remark 2 The reaching speed decreases gradually from a huge number when the state errors of the system are away from the surface in the exponential approach law. We know the crucial factor is the linear term. Considering the linear term in Eq. (42) can adjust the convergence rate of the system, we added a linear expression in terms of s to the dynamic formula u_1 of the STC algorithm, to improve the dynamic response of the higher-order term. In addition, the ST-SMC algorithm can effectively suppress the chattering problem, so the system can quickly reach the sliding mode surface.

The control scheme adopted in this study is shown in Fig. 2. After the feedback control process, the tracking state parameters r^*, λ^*, ϕ^*, γ^*, ψ^*, and V^* are finally obtained.

4.3 Parameter discussion

For the leap gliding trajectory, the reference drag trajectory is a continuous curve. However, the performance of the tracking controller varies along the entire time series. Taking GFT-SMC as an example (Fig. 3),

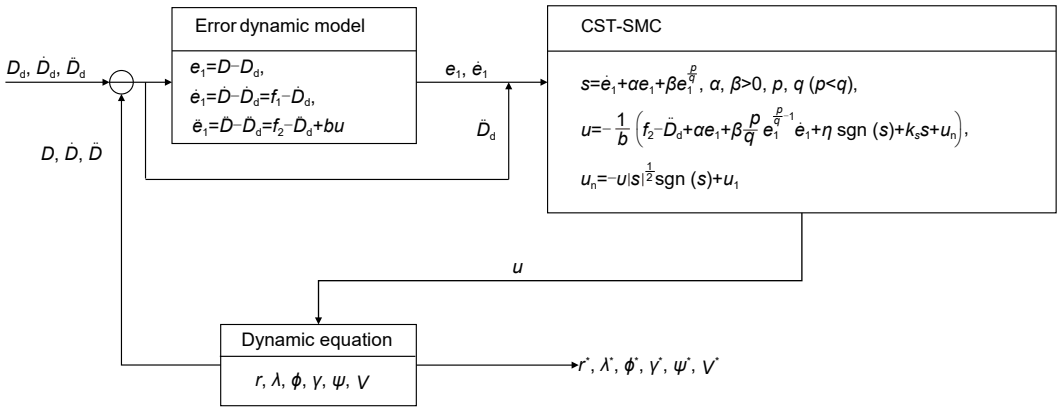

Fig. 2 A block diagram of the drag tracking control problem using CST-SMC

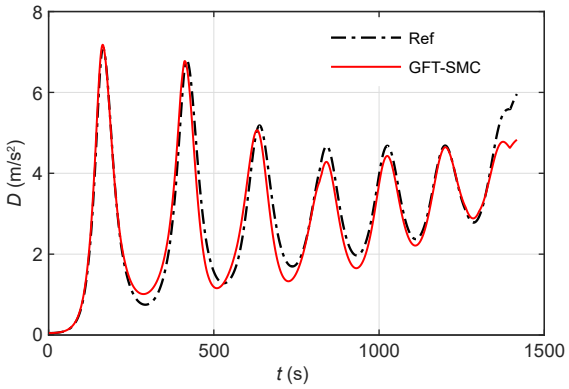

Fig. 3 Drag tracking profile of GFT-SMC. Ref represents the reference drag trajectory

the tracking results of the middle segment are not acceptable compared to those of the initial and ending segments. The reasons are as follows:

1. Adaptability of multi-parameters. The leap gliding flight has more severe and frequent state changes. Because the oscillation characteristics of the trajectory differ from those of cruise flight and quasi-equilibrium gliding flight, the constant gains cannot always meet the tracking requirements accurately along the total time series. Thus, adaptive parameters can be introduced to match the system changes. It is vital to determine the influence of every parameter on the system, to enable selection of feasible parameters. The parameters of controller Eq. (63) were analyzed. Increasing k_s could increase the velocity approaching the sliding surface without being too large. On the contrary, the gain η of the constant approaching term $\dot{s}=-\eta\,\mathrm{sgn}(s)$ needs to be small enough as s converges to zero in order to meet the lower terminal speed. α and β also have clear physical meanings, which determine mainly the convergence time in different phases. If the system states are far away from the origin points, β will play a major role in controlling convergence time, while α works mainly if the system nears the points. The purpose of adjusting α and β is to improve the approaching velocity as soon as possible. In the STC algorithm, parameters υ and ω can influence the steady-state error and eliminate chattering. k_2 can change the dynamic response of higher-order terms of the system. Before the parameters are decided, the magnitude and range need to be estimated according to the error system, and then every parameter needs to be modified carefully. In this study, the piecewise function was planned to reduce the drag tracking error in the whole tracking process.

2. Different controllers perform differently in the same system. By comparing the CST-SMC with traditional controllers, the advantages of CST-SMC were highlighted.

In addition, the CST-SMC proposed here theoretically can be applied to any nonlinear system models. However, considering the different characteristics among the models, the control results may be worse than those of the classical controllers, so it is not possible to guarantee that the performance is optimal for all nonlinear models. In this study, we considered the re-entry trajectory tracking control problems for a class of hypersonic gliding vehicles. Of course, in addition to the vehicle model (CAV-H, a generic high-performance common aero vehicle) (An et al., 2020) and its reference trajectory used in the simulation, CST-SMC is commonly used for other spacecraft and equilibrium gliding trajectories (such as the Mars entry trajectory). The above parameter discussion is crucial for designing

controller parameters rapidly, and provides a useful reference for development.

5 Simulation results

In this section, we will conduct four simulations: comparing tracking performance of the four controllers (L-SMC, GFT-SMC, ST-SMC, and CST-SMC) for a drag reference trajectory, comparing tracking performance of a PID controller and CST-SMC, verifying the robustness under the influence of parameter perturbation, and initial parameter measurement errors. The initial conditions and parameters of the controllers are shown in Tables 1 and 2, respectively. The CAV-H model was considered in the simulations.

Table 1 Initial conditions for hypersonic vehicle simulation

H (km)	λ (°)	ϕ (°)	γ (°)	ψ (°)	V (m/s)
80	0	−5	0	60	6000

In Table 2, for ST-SMC,

$$\begin{cases} \alpha_{ST}=0.05,\ \beta_{ST}=0.015,\ \upsilon_{ST}=0.0075, \\ \qquad\qquad 0\leqslant t\leqslant 420\ \text{s}, \\ \alpha_{ST}=0.001,\ \beta_{ST}=0.01,\ \upsilon_{ST}=0.002, \\ \qquad\qquad 420\ \text{s}<t\leqslant 1000\ \text{s}, \\ \alpha_{ST}=0.002,\ \beta_{ST}=0.005,\ \upsilon_{ST}=0.002, \\ \qquad\qquad t>1000\ \text{s}. \end{cases}$$

For CST-SMC,

$$\begin{cases} \alpha_{CST}=0.08,\ \beta_{CST}=0.05,\ \upsilon_{CST}=0.0075, \\ \quad \eta_{CST}=5\times10^{-8},\ k_{1CST}=2\times10^{-5},\quad 0\leqslant t\leqslant 400\ \text{s}, \\ \alpha_{CST}=0.001,\ \beta_{CST}=0.001,\ \upsilon_{CST}=0.002, \\ \quad \eta_{CST}=5\times10^{-8},\ k_{1CST}=0.4,\quad 400\ \text{s}<t\leqslant 500\ \text{s}, \\ \alpha_{CST}=0.001,\ \beta_{CST}=0.005,\ \upsilon_{CST}=0.002, \\ \quad \eta_{CST}=5\times10^{-8},\ k_{1CST}=0.05,\quad 500\ \text{s}<t\leqslant 800\ \text{s}, \\ \alpha_{CST}=0.00145,\ \beta_{CST}=0.002,\ \upsilon_{CST}=0.005, \\ \quad \eta_{CST}=5\times10^{-8},\ k_{1CST}=0.2,\quad t>800\ \text{s}. \end{cases}$$

5.1 Case 1: simulation without parameter perturbation

With the proposed control law Eq. (63), the simulation results without parameter perturbation are shown in Fig. 4. The tracking error of CST-SMC is clearly less than those of the other three controllers (Fig. 4h). A superior tracking performance is obvious as the drag acceleration (Fig. 4g) always moves along the desired profile, as with other longitudinal states such as altitude trajectory (Fig. 4a), velocity (Fig. 4c), and flight path angle (Fig. 4d). The lateral state errors (Fig. 4b) in the longitude-latitude plane are obvious in the process of tracking because of the poor fitting of the bank angle (Fig. 4e) and azimuth (Fig. 4f) profiles, but the terminal longitude error and latitude error are all less than 0.5°. This comparison of the four controllers demonstrates the superior tracking performance of the proposed method.

5.2 Case 2: simulation comparison with classical controller

As one of the most classical controllers, the PID controller has been widely applied in various control fields. In this study, we compared the CST-SMC with the PID controller, and the results are shown in Fig. 5. The following conclusions can be drawn:

1. The PID controller has just three control parameters, which is convenient for adjustment, but more difficult for obtaining appropriate parameters.

2. The PID controller with constant parameters or piecewise constant parameters cannot track the reference drag curve well. The tracking errors for serious states (Figs. 5a and 5b) and drag (Fig. 5c) are obvious in the corresponding figures. For better control results, it is important to develop an adaptive PID controller and further consider the problem of calculation efficiency.

3. Although the expression of the CST-SMC is not as simple as that of a PID controller, it has greater control, higher control precision, and other obvious advantages.

Table 2 Parameters of the controllers

Controller	c	η	k_s	α	β	p	q	υ	k_2	ω
L-SMC	0.002	5×10^{-8}	0.2	–	–	5	3	–	–	–
GFT-SMC	–	5×10^{-8}	0.2	0.0018	0.005	5	3	–	–	–
ST-SMC	–	–	–	α_{ST}	β_{ST}	5	3	υ_{ST}	0.2	5×10^{-6}
CST-SMC	–	η_{CST}	k_{1CST}	α_{CST}	β_{CST}	5	3	υ_{CST}	0.5	5×10^{-6}

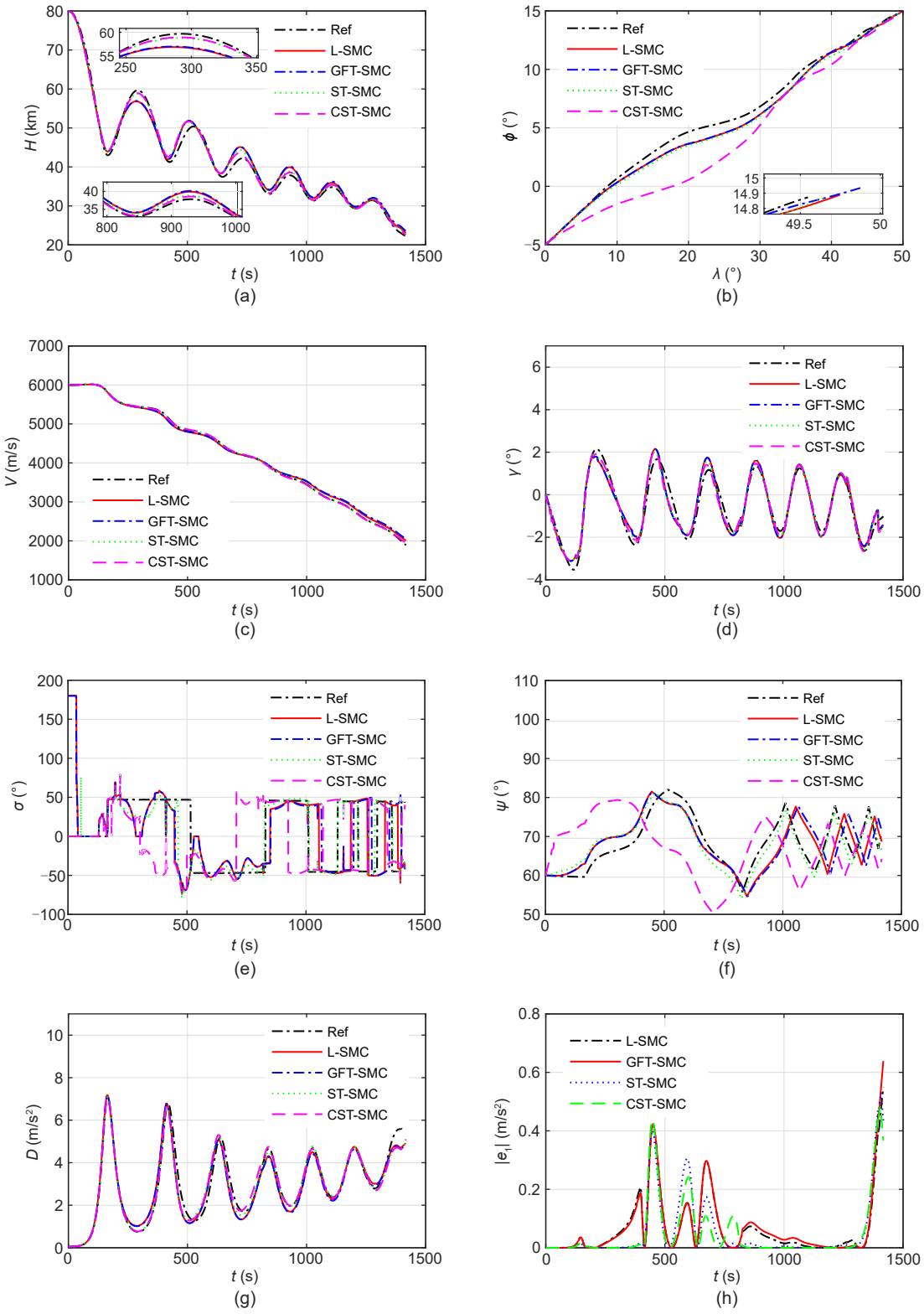

Fig. 4 Comparison of simulation results of the four controllers: (a) altitude trajectory profile; (b) land trajectory profile; (c) velocity profile; (d) flight path angle profile; (e) bank angle profile; (f) azimuth angle profile; (g) drag tracking profile; (h) drag tracking error

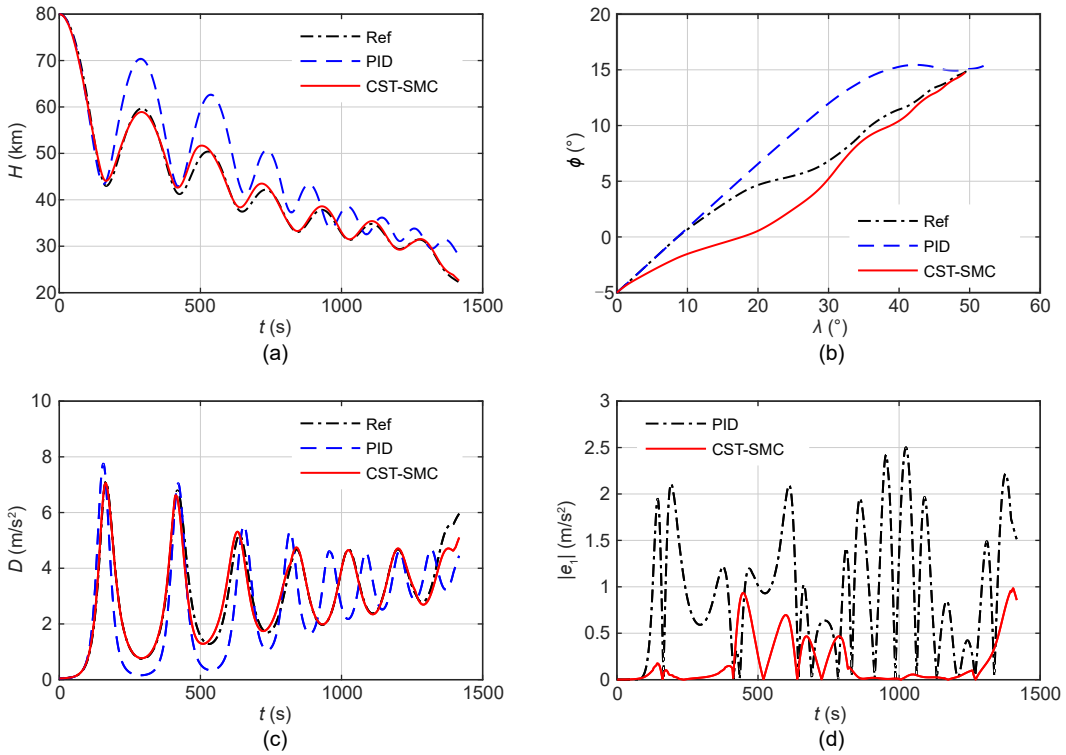

Fig. 5 Comparison of simulation results from PID and CST-SMC: (a) altitude tracking profile; (b) land trajectory tracking profile; (c) drag tracking profile; (d) drag tracking error

5.3 Case 3: simulation with parameter perturbation

Normally, the air density ρ, aerodynamic parameters B_{fn}, and lift-to-drag ratio $k_{L/D}$ will inevitably generate parameter perturbation due to the strict flight environment and high re-entry speed. Here, we consider constant parameter perturbation and stochastic parameter perturbation to verify the robustness of the proposed controllers. The constant and random parameter settings are shown in Table 3, where rand is a random number taken from [−1, 1].

Table 3 Settings of constant parameter perturbation and stochastic parameter perturbation

Item	ρ	B_{fn}	$k_{L/D}=C_L/C_D$
(A)	(1+0.15) ρ	(1+0.2) B_{fn}	(1+0.1) $k_{L/D}$
(B)	(1+0.15×rand) ρ	(1+0.2×rand) B_{fn}	(1+0.1×rand) $k_{L/D}$

(A) Constant parameter perturbation

The simulation results in Fig. 6 confirm that our proposed method has better tracking robustness for the reference states with constant parameter perturbation. Figs. 6a, 6b, and 6d show that the system has lower errors when using the CST-SMC, where the *Y*-axis is calculated by $E_i=\frac{1}{2}e_{1i}^2 (i=H, V, D)$, and e_{1i} represents the tracking error of i. The land trajectory is expressed by Fig. 6c, which shows the differences in the reference trajectory among all four controllers, but they all reach the terminal constraint position (50°, 15°) in finite time. Note that the bank angle produces severe tracking error, and thus the land trajectory is different.

(B) Stochastic parameter perturbation

Note that the altitude error (Fig. 7a) and speed error (Fig. 7b) of the L-SMC and GFT-SMC are several times higher than those of the proposed CST-SMC. Fig. 7d shows that, owing to the influence of stochastic parameter perturbation, the curves exhibit oscillation. Similarly, the system performs better using the CST-SMC method under stochastic parameter perturbation.

5.4 Case 4: simulation with the initial parameter measurement error influence

The settings of the initial parameter measurement errors are shown in Table 4. In setting 1, the altitude H and velocity V suffer a small disturbance; in

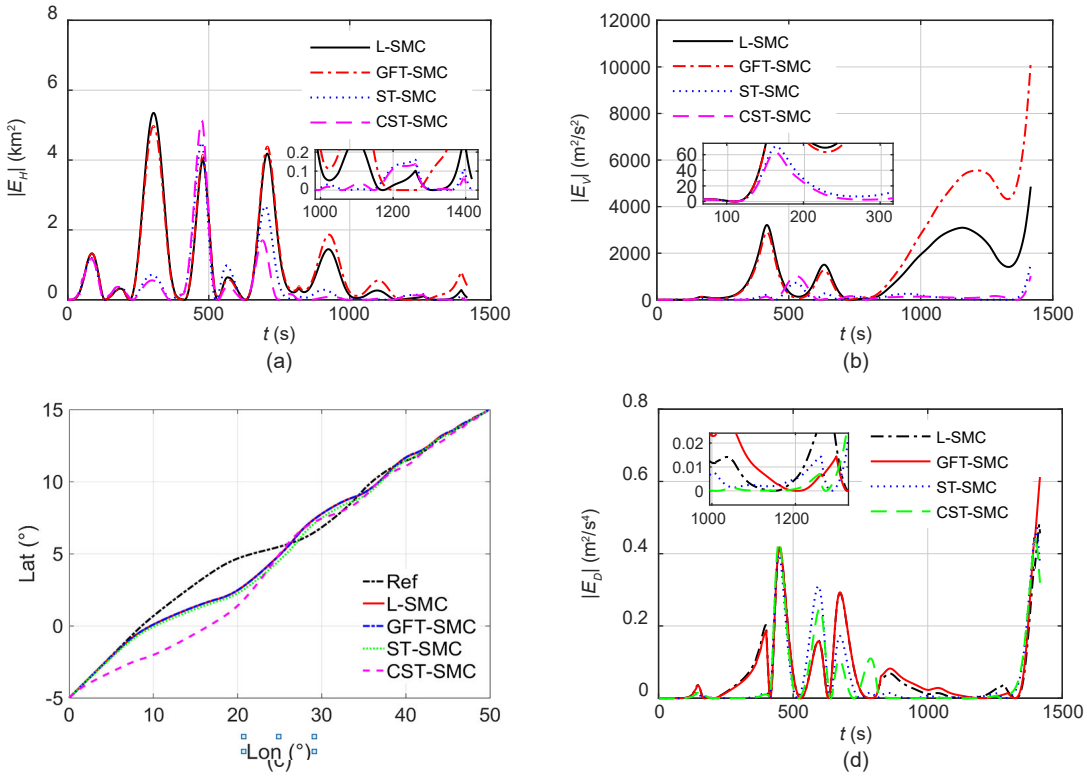

Fig. 6 Tracking results with constant parameter perturbation: (a) altitude tracking error; (b) velocity tracking error; (c) land trajectory profile; (d) drag tracking error

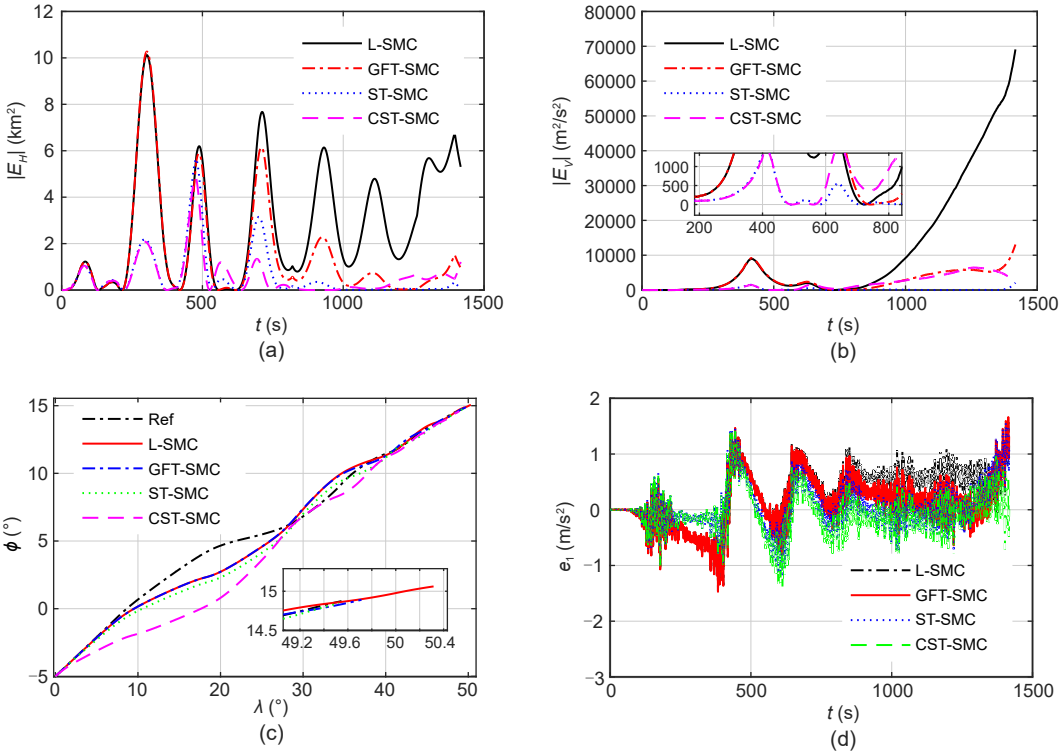

Fig. 7 Tracking results with stochastic parameter perturbation: (a) altitude tracking error; (b) velocity tracking error; (c) land trajectory profile; (d) drag tracking error

setting 2, the influence of changed lateral parameters will be examined; in setting 3, all the initial states will be disturbed.

From Figs. 8a and 8b, the curves of setting 1 and setting 3 have obvious errors due to the initial disturbances of altitude and velocity. Fig. 8c shows that the performance of our proposed controller is robust and insensitive to initial altitude and velocity measurement errors. The bank angle profile in Fig. 8d satisfies the constraint scope.

Based on the simulation results of the three cases, the proposed CST-SMC can adapt to different initial parameter measurement errors and ensures that hypersonic gliding vehicles can precisely track the reference trajectory under constraints. Moreover, the CST-SMC achieves faster convergence of the sliding surface in finite time and reduces the tracking errors compared with the other three controllers.

6 Conclusions

This study was concerned with the 3D trajectory tracking problem of hypersonic gliding vehicles. The reference trajectory was obtained by the predictor-corrector guidance method. The drag acceleration was chosen as the reference profile to be tracked and the bank angle as the control variable. Then, a CST-SMC based on the T-SM surface was proposed for guaranteeing the finite-time convergence of the drag tracking error even with parameter perturbation and initial parameter measurement uncertainties. We also deduced three traditional sliding mode controllers, the L-SMC, GFT-SMC, and ST-SMC, and compared their control performance with CST-SMC in simulations. The results showed that the CST-SMC has much better tracking performance than the other three controllers in the presence of various uncertainties, and has great application potential.

Table 4 Settings of the initial parameter measurement errors

Setting	H (km)	λ (°)	ϕ (°)	γ (°)	ψ (°)	V (m/s)
1	80−2	0	−5	0	60	6000+100
2	80	0−0.5	−5+0.5	0−0.005	60−0.05	6000
3	80+2	0−0.5	−5+0.5	0−0.5	60+1	6000+100

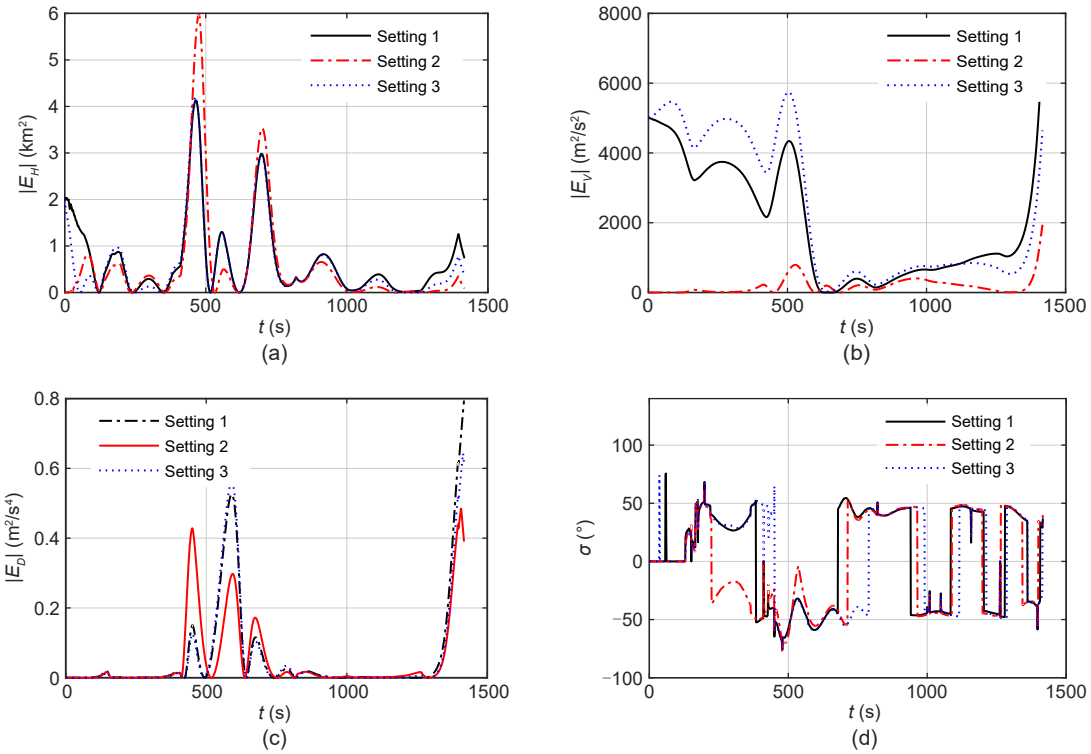

Fig. 8 Simulation results with the influence of initial parameter measurement uncertainties: (a) altitude tracking error; (b) velocity tracking error; (c) drag tracking error; (d) bank angle profile

Acknowledgments

This work is supported by the National Natural Science Foundation of China (No. 11972368) and the Natural Science Foundation of Hunan Province (No. 2021JJ10045), China.

Author contributions

Kai AN designed the research and processed the corresponding data. Zhen-yun GUO wrote the first draft of the manuscript. Wei HUANG and Xiao-ping XU helped to organize the manuscript. Kai AN and Wei HUANG revised and edited the final version.

Conflict of interest

Kai AN, Zhen-yun GUO, Wei HUANG, and Xiao-ping XU declare that they have no conflict of interest.

References

An H, Liu JX, Wang CH, et al., 2016. Disturbance observer-based antiwindup control for air-breathing hypersonic vehicles. *IEEE Transactions on Industrial Electronics*, 63(5): 3038-3049. https://doi.org/10.1109/TIE.2016.2516498

An K, Guo ZY, Xu XP, et al., 2020. A framework of trajectory design and optimization for the hypersonic gliding vehicle. *Aerospace Science and Technology*, 106:106110. https://doi.org/10.1016/j.ast.2020.106110

Awad A, Wang HP, 2016. Roll-pitch-yaw autopilot design for nonlinear time-varying missile using partial state observer based global fast terminal sliding mode control. *Chinese Journal of Aeronautics*, 29(5):1302-1312. https://doi.org/10.1016/j.cja.2016.04.020

Chen K, Liang WC, Liu MX, et al., 2020. Comparison of geomagnetic aided navigation algorithms for hypersonic vehicles. *Journal of Zhejiang University-SCIENCE A (Applied Physics & Engineering)*, 21(8):673-683. https://doi.org/10.1631/jzus.A1900648

Chen K, Liang WC, Zeng CZ, et al., 2021. Multi-geomagnetic-component assisted localization algorithm for hypersonic vehicles. *Journal of Zhejiang University-SCIENCE A (Applied Physics & Engineering)*, 22(5):357-368. https://doi.org/10.1631/jzus.A2000524

Du X, Li HY, Huang YC, 2015. Efficient nonlinear algorithm for drag tracking in entry guidance. *Procedia Engineering*, 99:1014-1026. https://doi.org/10.1016/j.proeng.2014.12.635

Farrell J, Sharma M, Polycarpou M, 2005. Backstepping-based flight control with adaptive function approximation. *Journal of Guidance, Control, and Dynamics*, 28(6):1089-1102. https://doi.org/10.2514/1.13030

Fiorentini L, Serrani A, Bolender MA, et al., 2009. Nonlinear robust adaptive control of flexible air-breathing hypersonic vehicles. *Journal of Guidance, Control, and Dynamics*, 32(2):402-417. https://doi.org/10.2514/1.39210

Fu SN, Lu TY, Yin J, et al., 2021. Rapid algorithm for generating entry landing footprints satisfying the no-fly zone constraint. *International Journal of Aerospace Engineering*, 2021:8827377. https://doi.org/10.1155/2021/8827377

Harpold JC, Graves Jr CA, 1979. Shuttle entry guidance. *Journal of the Astronautical Sciences*, 27(3):239-268.

Humaidi AJ, Hasan AF, 2019. Particle swarm optimization-based adaptive super-twisting sliding mode control design for 2-degree-of-freedom helicopter. *Measurement and Control*, 52(9-10):1403-1419. https://doi.org/10.1177/0020294019866863

Levant A, 1998. Robust exact differentiation via sliding mode technique. *Automatica*, 34(3):379-384. https://doi.org/10.1016/S0005-1098(97)00209-4

Li GH, Zhang HB, Tang GJ, 2015. Maneuver characteristics analysis for hypersonic glide vehicles. *Aerospace Science and Technology*, 43:321-328. https://doi.org/10.1016/j.ast.2015.03.016

Liu Z, Tan XM, Yuan RY, et al., 2015. Adaptive trajectory tracking control system design for hypersonic vehicles with parametric uncertainty. *Proceedings of the Institution of Mechanical Engineers, Part G: Journal of Aerospace Engineering*, 229(1):119-134. https://doi.org/10.1177/0954410014527251

Lu P, 2014. Entry guidance: a unified method. *Journal of Guidance, Control, and Dynamics*, 37(3):713-728. https://doi.org/10.2514/1.62605

Lu Q, Zhou J, 2017. LQR tracking guidance law for hypersonic vehicle. Proceedings of the 29th Chinese Control and Decision Conference, p.7090-7094. https://doi.org/10.1109/CCDC.2017.7978461

Moreno JA, Osorio M, 2012. Strict Lyapunov functions for the super-twisting algorithm. *IEEE Transactions on Automatic Control*, 57(4):1035-1040. https://doi.org/10.1109/TAC.2012.2186179

Sänger E, Bredt J, Ainring A, 1952. A Rocket Drive for Long Range Bombers. Government Printing Office, Washington, USA.

Truong TN, Vo AT, Kang HJ, 2021. A backstepping global fast terminal sliding mode control for trajectory tracking control of industrial robotic manipulators. *IEEE Access*, 9:31921-31931. https://doi.org/10.1109/ACCESS.2021.3060115

Tsien HS, Adamson TC, Knuth EL, 1952. Automatic navigation of a long range rocket vehicle. *Journal of the American Rocket Society*, 22(4):192-199. https://doi.org/10.2514/8.4467

Utkin V, 1977. Variable structure systems with sliding modes. *IEEE Transactions on Automatic Control*, 22(2): 212-222. https://doi.org/10.1109/TAC.1977.1101446

Wen YM, Wu ST, Hu NX, 2014. The analysis and design of control system for unpowered skipping-glide air vehicle in near space. Proceedings of the 33rd Chinese Control Conference, p.3703-3708. https://doi.org/10.1109/ChiCC.2014.6895555

Wu HN, Feng S, Liu ZY, et al., 2017. Disturbance observer based robust mixed H_2/H_∞ fuzzy tracking control for

hypersonic vehicles. *Fuzzy Sets and Systems*, 306:118-136. https://doi.org/10.1016/j.fss.2016.02.002

Xiu CB, Guo PH, 2018. Global terminal sliding mode control with the quick reaching law and its application. *IEEE Access*, 6:49793-49800. https://doi.org/10.1109/ACCESS.2018.2868785

Xu ML, Chen KJ, Liu LH, et al., 2012. Quasi-equilibrium glide adaptive guidance for hypersonic vehicles. *Science China Technological Sciences*, 55(3):856-866. https://doi.org/10.1007/s11431-011-4727-z

Yan BB, Dai P, Liu RF, et al., 2019. Adaptive super-twisting sliding mode control of variable sweep morphing aircraft. *Aerospace Science and Technology*, 92:198-210. https://doi.org/10.1016/j.ast.2019.05.063

Yu XH, Man ZH, 2009. Fast terminal sliding-mode control design for nonlinear dynamical systems. *IEEE Transactions on Circuits and Systems*, 49(2):261-264. https://doi.org/10.1109/81.983876

Zhang GG, Wang Y, Wang J, et al., 2020. Disturbance observer-based super-twisting sliding mode control for formation tracking of multi-agent mobile robots. *Measurement and Control*, 53(5-6):908-921. https://doi.org/10.1177/0020294020909126

Zhang YL, Chen KJ, Liu LH, et al., 2016. Entry trajectory planning based on three-dimensional acceleration profile guidance. *Aerospace Science and Technology*, 48:131-139. https://doi.org/10.1016/j.ast.2015.11.009

Zhao HW, Li R, 2020. Typical adaptive neural control for hypersonic vehicle based on higher-order filters. *Journal of Systems Engineering and Electronics*, 31(5):1031-1040. https://doi.org/10.23919/JSEE.2020.000077

Zhao PL, Chen WC, Yu WB, 2019. Analytical solutions for longitudinal-plane motion of hypersonic skip-glide trajectory. *Nonlinear Dynamics*, 96(3):1947-1969. https://doi.org/10.1007/s11071-019-04897-8

Zhao ZH, Yang J, Li SH, et al., 2016. Drag-based composite super-twisting sliding mode control law design for Mars entry guidance. *Advances in Space Research*, 57(12):2508-2518. https://doi.org/10.1016/j.asr.2016.03.036

Zong Q, Dong Q, Wang F, et al., 2015. Super twisting sliding mode control for a flexible air-breathing hypersonic vehicle based on disturbance observer. *Science China Information Sciences*, 58(7):1-15. https://doi.org/10.1007/s11432-015-5350-6